

Quantum Plasmonics with Quantum Dot-Metal Nanoparticle Molecules: Influence of the Fano Effect on Photon Statistics

A. Ridolfo, O. Di Stefano, N. Fina, R. Saija, and S. Savasta

Dipartimento di Fisica della Materia e Ingegneria Elettronica, Università di Messina, F. Stagno d'Alcontres 31, I-98166 Messina, Italy
(Received 13 April 2010; revised manuscript received 11 June 2010; published 20 December 2010)

We study theoretically the quantum optical properties of hybrid molecules composed of an individual quantum dot and a metallic nanoparticle. We calculate the resonance fluorescence of this composite system. Its incoherent part, arising from nonlinear quantum processes, is enhanced by more than 2 orders of magnitude as compared to that of the dot alone. The coupling between the two systems gives rise to a Fano interference effect which strongly influences the quantum statistical properties of the scattered photons: a small frequency shift of the incident light field may cause changes in the intensity correlation function of the scattered field of orders of magnitude. The system opens a good perspective for applications in active metamaterials and ultracompact single-photon devices.

DOI: 10.1103/PhysRevLett.105.263601

PACS numbers: 42.50.Pq, 42.50.Ar, 42.50.Dv, 71.35.Cc

Metal nanoparticles (MNP) have outstanding optical properties [1] that led to a revolution in physics, chemistry, material and life sciences [1,2]. Their ability to enhance and focus optical fields to spots much smaller than the diffraction limit stems from the occurrence of localized surface plasmons (LSP), i.e., collective wavelike motion of free electrons on the MNP surface. Bottom-up fabrication techniques of plasmonic nanoparticle clusters with unprecedented control are promising towards the realization of low-cost photonic nanodevices [3]. Plasmonics is leading to a huge number of applications such as ultrasensitive spectroscopy [4], nanoscale laser cavities (spaser) [5], and optical nanocircuits [6–8] that can merge electronics and photonics at the nanoscale. Logic elements for optical circuits require control over the interaction between single photons and individual optical emitters. Substantial advances towards the realization of solid state quantum optical devices have been made by coupling single quantum dots (QDs) to high-finesse optical cavities [9,10]. An inherent limitation of these systems is that the size of the cavity has to be at least half wavelength and practically much larger owing to the presence of mirrors or of a surrounding photonic crystal [9,10]. In this context, individual MNP can be exploited as nanoscale cavities [5] offering a route to size reductions. Optical nonlinearities enable photon-photon interaction and lie at the heart of photonic quantum-information [10–12], and single-photon switching [8,13]. While many plasmonic features can be described within the classical theory of electromagnetism, the nonlinear optical properties of individual quantum emitters [14,15] necessitate a quantum treatment of the optical field [16,17]. Moreover, in order to investigate the possible use of these artificial molecules as devices for the control of individual light quanta in optical nanocircuits, a quantum treatment of the radiation field is required.

Here we investigate the quantum optical properties of a QD-MNP hybrid artificial molecule. We find that the inelastic part of resonance fluorescence, arising from nonlinear quantum processes, increases by more than 2 orders of magnitude with respect to the uncoupled dot value. These quantum nonlinear processes are at the basis of many important quantum optical effects such as optical squeezing [17], nonclassical photon correlations [16]. The obtained scattering spectra display an asymmetric Fano resonance. The Fano effect, ubiquitous in the spectroscopy of atoms and solids [18], arises when quantum interference takes place between two competing optical pathways and is particularly important in the interpretation of electronic transport and optical spectra in semiconductors and coupled MNPs [3,19]. We show that single-photon nonlinearities of the quantum emitter enable the control of the Fano resonance with the arrival of a single-photon. We consider a spherical QD interacting with a spherical MNP of radius r_m , separated by a distance R (see Fig. 1). There is no direct tunneling between the MNP and the SQD ($R - r_m - r_{\text{QD}} > 2$ nm, being r_{QD} the QD radius). The coupling

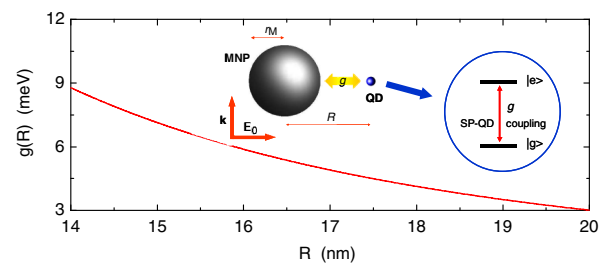


FIG. 1 (color online). Interaction between a quantum dot and a silver nanoparticle: the applied electromagnetic field induces a polarization that causes dipole-dipole coupling. States $|g\rangle$ and $|e\rangle$ are coupled via the localized surface plasmon dipole mode with a strength g . Dependence of the coupling g on the metallic nanoparticle-quantum dot distance R .

mechanism due to dipole-dipole interaction at wavelengths around the SP dipole resonance is largely independent on the geometric details of the MNP, as verified by accurate scattering calculations beyond the dipole approximation [1,20]. The quantum dot is modeled as a two level system with a dipole moment μ , that is a good approximation when studying optical processes at frequencies resonant with the lowest energy excitonic transition [16]. The artificial molecule is excited by an applied electromagnetic field $E_i = E_0 e^{-i\omega_i t} + \text{c.c.}$ polarized along the system axis. The positive-frequency component of the electric field oscillating as $\exp(-i\omega t)$ felt by a quantum emitter, $E_{\text{QD}} = E_0 + E_m$ is due to the superposition of the input field E_0 and the field $E_m = (s_\alpha P_m / 4\pi\epsilon_0\epsilon_b R^3)$, arising from the induced polarization of the MNP [14] $P_m = 4\pi\epsilon_0\epsilon_b\beta r_m^3(E_0 + s_\alpha P_x / 4\pi\epsilon_0\epsilon_b R^3)$, where $s_\alpha = 2$ for an applied electrical field parallel to \mathbf{R} ($s_\alpha = -1$ for a field orthogonal to \mathbf{R}). The entire system is embedded in a dielectric medium with constant permittivity ϵ_b . $P_x = \mu\langle\sigma\rangle$ is the positive-frequency component of the QD polarization, being $\langle\sigma\rangle$ the expectation value of the lowering transition operator $\sigma = |g\rangle\langle e|$. The frequency-dependent complex coefficient $\beta = (\epsilon_m(\omega) - \epsilon_b) / (2\epsilon_b + \epsilon_m(\omega))$ determines the SP dipole resonance frequency ω_{sp} satisfying $\text{Re}[\epsilon_m(\omega_{\text{sp}})] = -2\epsilon_b$. Performing the first order expansion of $\text{Re}[\epsilon_m(\omega)]$ around ω_{sp} , β can be well approximated by the complex Lorentzian $\beta \cong 3i\epsilon_b\eta / [i(\omega_{\text{sp}} - \omega) + \gamma_{\text{sp}}/2]$, with $\eta^{-1} = d\text{Re}[\epsilon_m(\omega)] / d\omega|_{\omega=\omega_{\text{sp}}}$ and $\gamma_{\text{sp}} = 2\eta\text{Im}[\epsilon_m(\omega_{\text{sp}})]$. This approximation enables the description of SP resonances within the quasi-mode approach, largely exploited in the framework of cavity-quantum electrodynamics (CQED) [17,21]. The full quantum dynamics of the coupled nanosystem can be derived from the following master equation for the density operator, $\dot{\rho} = \frac{i}{\hbar}[\rho, H_S] + \mathcal{L}_x + \mathcal{L}_{\text{sp}}$. The system Hamiltonian is $H_S = H_0 + H_{\text{int}} + H_{\text{drive}}$ with $H_0 = \hbar\omega_{\text{sp}}a^\dagger a + \hbar\omega_x\sigma^\dagger\sigma$, being a the Bosonic destruction operator describing the SP-field mode and $\hbar\omega_x$ the energy of the QD excitonic transition. The Hamiltonian term describing the interaction between the QD exciton and the quantized SP field, in the rotating wave approximation reads $H_{\text{int}} = i\hbar g(a^\dagger\sigma - a\sigma^\dagger)$, where $\hbar g = \mu\mathcal{E}$, being $i\mathcal{E}a = \hat{E}_m^+$ the positive-frequency electric field operator at the QD position. The system excitation by a classical input field can be described by $H_{\text{drive}} = -E_0(\chi a^\dagger + \chi^* a) - \mu E_0(\sigma^\dagger + \sigma)$. The Markovian interaction with reservoirs determining the decay rates γ_x and γ_{sp} for the QD exciton and the SP mode, respectively, is described by the Liouvillian terms [17], $\mathcal{L}_i = (\gamma_i/2)(2d_i\rho d_i^\dagger - d_i^\dagger d_i\rho - \rho d_i^\dagger d_i)$, with $i = x, \text{sp}$, being $d_x = \sigma$ and $d_{\text{sp}} = a$. Starting from the master equation, the coupled equations of motion for the SP-field expectation values $\langle a \rangle \equiv \text{Tr}[a\rho]$ and for the emitter transition-operator determining the QD polarization $\langle \sigma \rangle \equiv \text{Tr}[\sigma\rho]$ can be obtained. The equation of motion for the exciton operator expectation value $\langle \sigma \rangle$ is

coupled to higher-order expectation values. The dynamics is solved by representing the photon operators on a basis of Fock number states. At steady state, the equation of motion for $\langle a \rangle$ can formally be solved, $\langle a \rangle = (g\langle\sigma\rangle + i\chi E_0/\hbar)/D(\omega)$, with $D(\omega) = i(\omega_{\text{sp}} - \omega) + \gamma_{\text{sp}}/2$. Equating the obtained electric field expectation value $E_m = i\mathcal{E}\langle a \rangle$ with E_m , we obtain, $\mathcal{E} = \sqrt{3\hbar\eta r_m^3/4\pi\epsilon_0}(s_\alpha/R^3)$ and $\chi = \epsilon_b\sqrt{12\pi\hbar\eta\epsilon_0 r_m^3}$. Figure 1 displays the dependence of g on the QD-MNP distance R . Throughout the Letter we use a dipole moment $\mu = er_0$ with $r_0 = 0.7$ nm (corresponding to 33.62 Debye), being e the electron charge and $\epsilon_b = 3$. In the following we use for the QD transition a linewidth $\gamma_x = 50$ μeV . We consider a silver MNP whose frequency-dependent dielectric permittivity is taken from Ref. [22]. Calculations yield SP dipole energy resonance $\omega_{\text{sp}} = 2887.73$ meV, and a corresponding linewidth $\gamma_{\text{sp}} = 53.28$ meV. Comparing the classical expression for the MNP polarization P_m with the steady-state result for $\langle a \rangle$, we obtain $P_m = \chi\langle a \rangle$. After the determination of \mathcal{E} and χ , a precise theoretical framework for nonperturbative quantum plasmonics is established. We calculate the Rayleigh scattering adopting the standard method which is valid when the size of the scattering objects is much smaller than the wavelength of incident light [14]. In this case the scattering intensity is proportional to $I_s = \langle \hat{P}^- \hat{P}^+ \rangle$, where $\hat{P}^+ = \chi a + \mu\sigma$ is the total polarization operator and $\hat{P}^- = (\hat{P}^+)^\dagger$. It is worth noticing that the scattered intensity contains a coherent part $I_s^{\text{coh}} = |\langle \hat{P}^+ \rangle|^2$ as well as incoherent contributions with the frequency of the scattered photons not necessarily coincident with that of incident light $I_s^{\text{incoh}} = \langle \hat{P}^-, \hat{P}^+ \rangle \equiv I_s - I_s^{\text{coh}}$. Figure 2(a) displays scattering spectra as function of the frequency of the incidence light obtained for different QD-MNP distances R as indicated in the panel. The spectra in Fig. 2(a) have been calculated in the limit of very low-excitation intensity, where the excitonic populations $\langle \sigma^\dagger\sigma \rangle \ll 1$. At $R = 14$ nm a Fano-like lineshape around the QD transition energy ω_x is evident. For a particular input frequency the scattered light is highly suppressed, while at slightly lower energy an enhancement of scattering due to constructive interference can be observed. For comparison the plot at $R = 14$ nm shows the scattering spectrum in the absence of the QD (dash-dotted line). Increasing the distance R , the Fano resonance narrows, due to the reduction of the MNP induced broadening of the QD linewidth. While at $R = 18$ nm the destructive interference remains almost complete, at larger distances ($R = 25$ nm), the Fano interference effect lowers and the suppression as well as the increase of the scattered light are reduced. Figure 2(b) displays scattering spectra obtained for QDs with different excitonic energy levels. In particular, each panel corresponds to different exciton-SP detunings $\Delta = \omega_x - \omega_{\text{sp}}$. Interestingly, the interference effect determining a strong suppression of scattering at specific wavelengths of the input field requires no special tuning unlike analogous

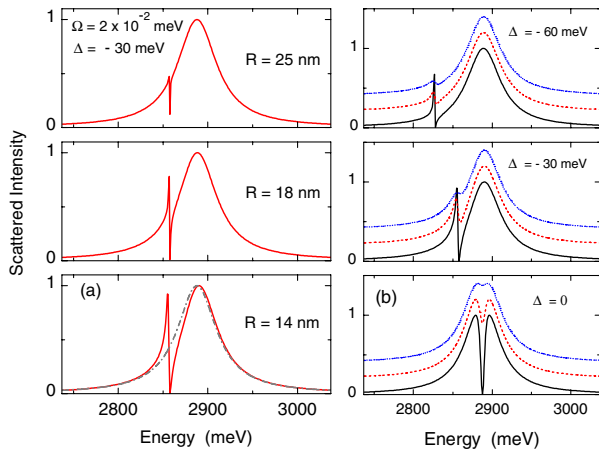


FIG. 2 (color online). (a) Scattered light intensity spectra (red continuous line) calculated for different QD-MNP distances R at low density excitation power. For $R = 14$ nm, the scattered light without the presence of the QD (dot-dashed line) is also plotted. (b) Spectra calculated at $R = 14$ nm. Each panel shows calculations for a specific exciton-SP energy detuning (Δ) indicated in the figure. The black continuous line describes plots obtained for an input intensity field $\Omega = 0.02$ meV (corresponding to a photon flux $\Phi = 1.75 \mu\text{m}^{-2} \text{ps}^{-1}$), the red short-dashed line plots obtained at $\Omega = 0.4$ meV ($\Phi = 700 \mu\text{m}^{-2} \text{ps}^{-1}$), and the blue short-dotted line plots at $\Omega = 1$ meV. Plots are peak normalized. The plot at $\Omega = 0.4$ meV was vertically shifted by 0.2, the one at $\Omega = 1$ meV by 0.4.

effects in CQED. While SPs supported by the MNP can be described as harmonic oscillators, the single QD displays nonlinearities at single-photon level. Panel 2b puts forward the dependence of light scattering on the intensity of the input field. The continuous lines describe low-field spectra obtained for a Rabi energy $\Omega = 2\mu E_0 = 2 \times 10^{-2}$ meV. Increasing the input field to $\Omega = 0.4$ meV, saturation effects appear (dashed line). At $\Omega = 1$ meV saturation is almost complete. The hybrid artificial molecule thus behaves as a frequency-dependent saturable scatterer. The output scattered light may be separated into coherent and incoherent parts. The coherent part is due to the elastic Rayleigh scattering: $\omega_s = \omega_i$. The incoherent part originates from the combination of nonlinear interactions and quantum fluctuations and cannot be described in a semiclassical context [17]. For low incident light intensities elastic scattering dominates, whereas for higher incident light intensities two-photon processes with $\omega_s + \omega_{s'} = 2\omega_i$ take place with the energies of scattered photons ω_s and $\omega_{s'}$ not necessarily equal to ω_i . The steady-state fluorescence emission spectra reads, $S(\omega_s) = \lim_{t \rightarrow \infty} 2 \text{Re} \int_0^\infty \langle P^-(t), P^+(t+\tau) \rangle e^{i\omega_s \tau} d\tau$. Two-time correlation can be calculated by exploiting the quantum regression theorem [17]. Figure 3(a) displays the incoherent part of the emitted intensity as a function of the input field for three different excitonic energy levels. Calculations have been performed for a frequency of the incident field $\omega_i = \omega_x$. The obtained results show that the MNP is able to strongly influence resonant quantum optical nonlinear

processes. Calculations have been performed considering a QD-MNP distance $R = 14$ nm. At resonance ($\Delta = 0$) we find an enhancement of a factor ~ 260 with respect to the QD incoherent emission in the absence of the MNP. The enhancement is the result of two different competing processes: (i) the enhancement of the QD emission due to the SP-increased density of photon modes; (ii) the quenching of the emitted light due to the losses induced by the MNP. Figure 3(b) displays the resonance fluorescence spectra (the incoherent part) as function of the detection frequency for different excitation powers, $\Omega = 0.2$ meV (short-dotted line), $\Omega = 0.4$ meV (short-dashed line) and $\Omega = 1$ meV (continuous line). It is seen that, with the increasing driving field intensity, the single-peak spectrum around $\omega_s = \omega_x$ is transformed into the three-peak Mollow spectrum [16]. The side peaks display a splitting significantly larger as compared to that for the uncoupled QD, owing to the SP induced enhancement of g , thus allowing a better filtering of the strong elastic component. The enhanced nonlinear optical response of an individual emitter leads to pronounced modifications of photon statistics that cannot be captured by only considering average intensities, but appears in higher-order correlations of the emitted and scattered fields. Specifically, we focus on the normalized steady-state second-order correlation functions $g^{(2)}$ for the scattered field which for a stationary process can be expressed in terms of the total polarization operators as $g^{(2)}(\tau) = \langle \hat{P}^-(t) \hat{P}^-(t+\tau) \hat{P}^+(t+\tau) \hat{P}^+(t) \rangle / |\langle \hat{P}^- \hat{P}^+ \rangle|^2$. Figure 4(a) shows the normalized second-order correlation functions for scattered photons calculated at low excitation power ($\Omega = 0.02$ meV) for two specific frequencies of the driving field indicated by arrows in the inset. The inset displays a detail of the low-excitation power scattering spectrum obtained for $\Delta = -60$ meV. The continuous line in Fig. 4(a) shows a huge bunching effect. It can be explained as follows: scattering of individual photons at this frequency is highly suppressed due to the Fano destructive interference, but when two photons are incident

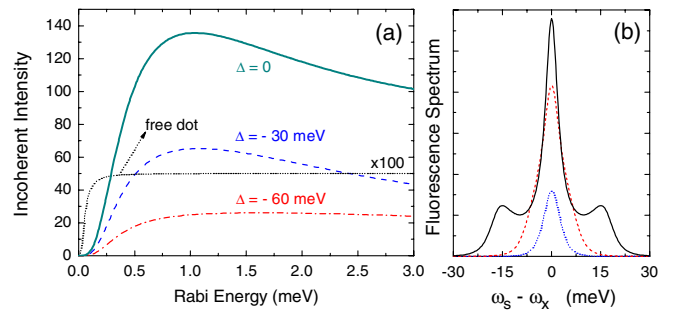


FIG. 3 (color online). (a) Incoherent intensity emission as function of the driving field intensity obtained for different exciton-SP detunings. The black short-dotted line describes the QD incoherent emission in the absence of the MNP. (b) Resonance fluorescence spectra: intensity of the scattered field as a function of the detected frequency calculated at three different pump intensities.

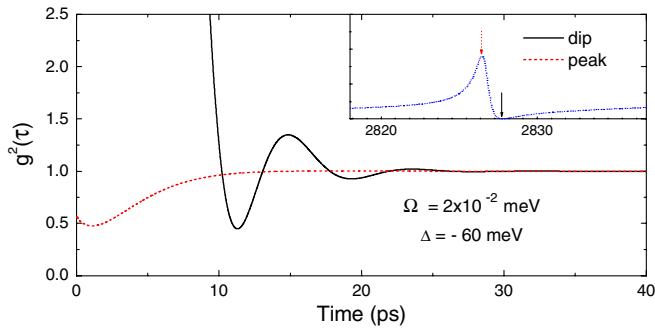


FIG. 4 (color online). (a) Normalized second-order correlation functions for the scattered field calculated at low-excitation power for two specific frequencies of the driving field indicated by arrows in the inset. The inset displays a detail of the low-excitation power scattering spectrum.

simultaneously the transition saturates, so that pairs have a much larger probability of scattering. For delay times among the two detection events larger than the exciton decay rate, $g^{(2)}(\tau) \rightarrow 1$, which is the standard level for coherent classical light. The dotted line in Fig. 4(a) describes the second-order correlation function $g^{(2)}(\tau)$ obtained fixing the frequency of the driving field at the Fano-peak corresponding to constructive interference. In this case saturation (induced by the photon pair) suppresses the Fano-peak determining a lowering of two-photon scattering which causes a dropping of $g^{(2)}(\tau)$ below the classical level (antibunching effect). The Fano resonance displayed by the MNP-QD system thus is able to affect dramatically the photon-statistics of scattered light: a small variation of the excitation frequency determines a variation of $g^{(2)}(0)$ for scattered light beyond 3 orders of magnitude. A greater degree of control over the scattered light (single-photon switch) can be achieved by considering a multilevel emitter, such as the three-level configuration [8]. If one additional state $|s\rangle$ is resonantly coupled to state $|e\rangle$ by a coherent control beam, the arrival of a single-photon “gate” pulse will cause the transition $|g\rangle \rightarrow |e\rangle \rightarrow |s\rangle$, disabling the Fano effect. A subsequent signal photon will be scattered according to the dashed dotted curve in Fig. 2(a). In the absence of the single-photon gate, the scattering of a signal photon at wavelength tuned at the Fano minimum will be highly suppressed.

The hybrid system here investigated is in experimental reach. QD nanocrystals emitters are promising candidates [23]. The photoluminescence enhancement of CdSe QDs on gold colloids has been demonstrated [24]. For example, chemically synthesized CdSe QDs can be spin-coated on a flat glass substrate with silver or gold nanoparticles [25] or they can be coupled in a fully controlled way with the metallic tip of a near-field apertureless optical microscope [26]. Self-assembled QDs, which can display a very high optical quality could also be exploited. Recently, hybrid structures consisting of a quantum dot and a metal nanoparticle joined by a biolinker have been assembled and

studied [27]. The Fano resonance, as well as the Fano-induced photon statistics occurs over a very large bandwidth (see Fig. 2). The effects here described can also be observed with quantum emitters displaying significantly larger spectral broadening if $\gamma_x \ll \gamma_{sp}$. For distances $R = 14$ nm, quantum emitters with dipole moments lower by 1 order of magnitude still work. One key feature of the proposed photon correlation measurements is that, thanks to the Fano effect, they do not require filtering out the dominant elastic component, which makes so difficult this kind of experiments [16]. The intriguing single-photon control of the Fano effect here described provides indications that these systems could be used as ultracompact building blocks in quantum-information technology, and for single-photon devices. This artificial hybrid molecule can be viewed as a promising flexible ultracompact unit. It can be also used as a building block to construct optically controllable plasmonic metamaterials [28], or to replace microcavities in arrays of nonlinear optical systems [29].

-
- [1] S. A. Maier, *Plasmonics: Fundamentals and Applications* (Springer, New York, 2007).
 - [2] H. A. Atwater, *Sci. Am.* **56**, (2007).
 - [3] J. A. Fan *et al.*, *Science* **328**, 1135 (2010).
 - [4] J. F. Li *et al.*, *Nature (London)* **464**, 392 (2010).
 - [5] M. A. Noginov *et al.*, *Nature (London)* **460**, 1110 (2009).
 - [6] E. Ozbay *et al.*, *Science* **311**, 189 (2006).
 - [7] N. Engheta, *Science* **317**, 1698 (2007).
 - [8] D. E. Chang *et al.*, *Nature Phys.* **3**, 807 (2007).
 - [9] J. P. Reithmaier *et al.*, *Nature (London)* **432**, 197 (2004); K. Hennessy *et al.*, *Nature (London)* **445**, 896 (2007).
 - [10] I. Fushman *et al.*, *Science* **320**, 769 (2008).
 - [11] C. Monroe, *Nature (London)* **416**, 238 (2002).
 - [12] Q. Turchette *et al.*, *Phys. Rev. Lett.* **75**, 4710 (1995).
 - [13] K. M. Birnbaum *et al.*, *Nature (London)* **436**, 87 (2005).
 - [14] W. Zhang, A. O. Govorov, and G. W. Bryant, *Phys. Rev. Lett.* **97**, 146804 (2006).
 - [15] R. Artuso and G. Bryant, *Nano Lett.* **8**, 2106 (2008).
 - [16] E. B. Flagg *et al.*, *Nature Phys.* **5**, 203 (2009).
 - [17] M. O. Scully and M. S. Zubairy, *Quantum Optics* (Cambridge University Press, Cambridge, England, 1997) 1st ed.
 - [18] See e.g. M. Kroner *et al.*, *Nature (London)* **451**, 311 (2008).
 - [19] N. Liu *et al.*, *Nature Mater.* **8**, 758 (2009).
 - [20] S. Savasta *et al.*, *ACS Nano* **4**, 6369 (2010).
 - [21] D. J. Bergman and M. I. Stockman, *Phys. Rev. Lett.* **90**, 027402 (2003).
 - [22] P. Johnson and R. Christy, *Phys. Rev. B* **6**, 4370 (1972).
 - [23] V. I. Klimov *et al.*, *Science* **290**, 314 (2000).
 - [24] O. Kulakovich *et al.*, *Nano Lett.* **2**, 1449 (2002).
 - [25] A. V. Akimov *et al.*, *Nature (London)* **450**, 402 (2007).
 - [26] S. Kühn *et al.*, *Phys. Rev. Lett.* **97**, 017402 (2006).
 - [27] Y. Jin and X. Gao, *Nature Nanotech.* **4**, 571 (2009).
 - [28] S. Zhang *et al.*, *Phys. Rev. Lett.* **101**, 047401 (2008).
 - [29] I. Carusotto *et al.*, *Phys. Rev. Lett.* **103**, 033601 (2009).